Cell

A Vitamin D Receptor/SMAD Genomic Circuit Gates Hepatic Fibrotic Response

Ning Ding,[1] Ruth T. Yu,[1] Nanthakumar Subramaniam,[3] Mara H. Sherman,[1] Caroline Wilson,[3] Renuka Rao,[3] Mathias Leblanc,[1] Sally Coulter,[3] Mingxiao He,[1] Christopher Scott,[4] Sue L. Lau,[4] Annette R. Atkins,[1] Grant D. Barish,[1] Jenny E. Gunton,[4] Christopher Liddle,[3] Michael Downes,[1,*] and Ronald M. Evans[1,2,*]
[1]Gene Expression Laboratory
[2]Howard Hughes Medical Institute
Salk Institute for Biological Studies, La Jolla, CA 92037, USA
[3]The Storr Liver Unit, Westmead Millennium Institute and University of Sydney, Westmead Hospital, Westmead, New South Wales 2145, Australia
[4]Diabetes and Transcription Factors Group, Garvan Institute of Medical Research, Darlinghurst, Sydney, New South Wales 2010, Australia
*Correspondence: downes@salk.edu (M.D.), evans@salk.edu (R.M.E.)
http://dx.doi.org/10.1016/j.cell.2013.03.028

SUMMARY

Liver fibrosis is a reversible wound-healing response involving TGFβ1/SMAD activation of hepatic stellate cells (HSCs). It results from excessive deposition of extracellular matrix components and can lead to impairment of liver function. Here, we show that vitamin D receptor (VDR) ligands inhibit HSC activation by TGFβ1 and abrogate liver fibrosis, whereas *Vdr* knockout mice spontaneously develop hepatic fibrosis. Mechanistically, we show that TGFβ1 signaling causes a redistribution of genome-wide VDR-binding sites (VDR cistrome) in HSCs and facilitates VDR binding at SMAD3 profibrotic target genes via TGFβ1-dependent chromatin remodeling. In the presence of VDR ligands, VDR binding to the coregulated genes reduces SMAD3 occupancy at these sites, inhibiting fibrosis. These results reveal an intersecting VDR/SMAD genomic circuit that regulates hepatic fibrogenesis and define a role for VDR as an endocrine checkpoint to modulate the wound-healing response in liver. Furthermore, the findings suggest VDR ligands as a potential therapy for liver fibrosis.

INTRODUCTION

Hepatic fibrosis, defined by excessive accumulation of extracellular matrix (ECM) and resultant loss of pliability and liver function, is the result of wound-healing responses triggered by either acute or chronic liver injury (Bataller and Brenner, 2005; Hernandez-Gea and Friedman, 2011; Lee and Friedman, 2011). The main causes of liver injury leading to fibrosis in industrialized countries include chronic hepatitis virus (hepatitis B virus/hepatitis C virus) infection, alcohol abuse, and, increasingly, nonalcoholic steatohepatitis (Friedman, 1999, 2003; Friedman and Bansal, 2006; Siegmund et al., 2005). With persistent injury, there is progressive deposition of fibrillar collagens, eventually leading to parenchymal nodules surrounded by collagen bands, the histological signature of hepatic cirrhosis (Bataller and Brenner, 2005; Friedman, 2003).

Chronic liver disease and cirrhosis represent a major global health concern (Bataller and Brenner, 2005). In Australia and the United Kingdom, chronic liver disease is the fifth most common cause of death, after heart disease, cancer, stroke, and chest disease (Williams, 2006). In the United States, they are ranked as the eighth most common cause of mortality (Kim et al., 2002). Currently, no antifibrotic therapies for chronic liver disease have been approved by the Food and Drug Administration (Cohen-Naftaly and Friedman, 2011), and where the underlying cause of the liver disease cannot be ameliorated, therapeutic options are limited to addressing the consequent complications, such as portal hypertension, hepatocellular carcinoma, and liver failure. Therefore, a greater understanding of molecular mechanisms regulating the hepatic fibrogenic response in liver is needed for the identification of novel targets for successful antifibrotic therapies.

The central players in liver fibrosis are nonparenchymal cells such as hepatic stellate cells (HSCs) (Bataller and Brenner, 2005; Bouwens et al., 1992), which are the main producers of ECM (Friedman, 2008; Friedman et al., 1985; Reynaert et al., 2002). In the healthy liver, HSCs are retinoid (vitamin A) storage cells located in the space of Disse, between the sinusoidal endothelium and hepatocytes (Friedman, 2008). Following injury, paracrine stimuli cause HSCs to undergo dramatic phenotypic changes (in a process called activation), whereby they exhibit proliferation, contractility, and loss of retinoid stores, accompanied by secretion of chemokines, cytokines, and pathological ECM components (Friedman, 2008; Geerts, 2001). While the precise mechanisms regulating this process have yet to be elucidated, transforming growth factor (TGF) β1 signaling is recognized as one of the most potent profibrotic pathways

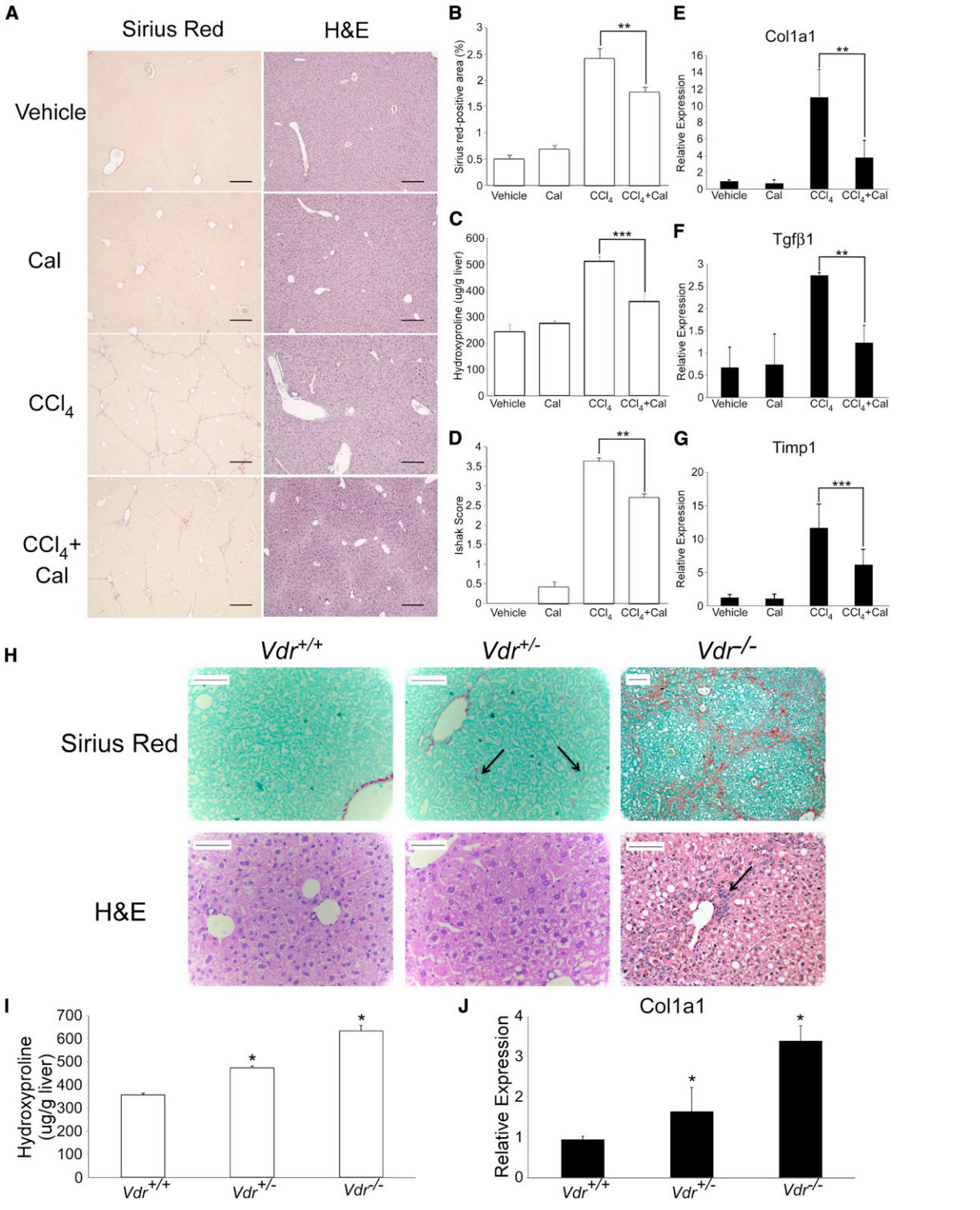

Figure 1. Systemic Administration of Calcipotriol Attenuates Liver Fibrosis in CCl_4-Treated Mice, whereas Genetic Abrogation of *Vdr* Results in Spontaneous Liver Fibrosis

(A) Livers from 4-week-treated C57BL/6J mice (vehicle [DMSO, n = 3], carbon tetrachloride [CCl_4, 0.5 ml/kg IP, n = 6], calcipotriol [Cal, 20 μg/kg oral gavage, n = 3], and CCl_4 plus calcipotriol [n = 6]) stained with Sirius red (left) and hematoxylin and eosin (H&E, right). Scale bar, 200 μm.

(B–D) Fibrosis quantified by (B) Sirius red staining, (C) hydroxyproline content, and (D) H&E staining (Ishak score). Asterisks denote statistically significant differences (Student's unpaired t test: **p < 0.01; ***p < 0.001).

(legend continued on next page)

responsible for ECM synthesis (Breitkopf et al., 2006; Inagaki and Okazaki, 2007).

TGFβ is a multifunctional cytokine with profound effects on cell division, differentiation, migration, adhesion, organization, and death. There are three major isoforms of TGFβ (TGFβ1, TGFβ2, and TGFβ3), and TGFβ1 is the principal isoform implicated in liver fibrosis (Inagaki and Okazaki, 2007). Following liver injury, TGFβ1, derived from both paracrine and autocrine sources, binds to type I and type II serine/threonine receptor kinases on the cell surface of HSCs (Inagaki and Okazaki, 2007). Subsequently, its downstream effectors SMAD2 and SMAD3 are phosphorylated and released into the cytosol, where they form a complex with SMAD4. This SMAD complex can then translocate into the nucleus, recognize SMAD-binding elements (SBE) on the genome, and directly regulate target genes (Feng and Derynck, 2005; Massagué et al., 2005). Thus, deciphering the TGFβ/SMAD transcriptional network in HSCs and understanding how it can be controlled by extracellular and intracellular factors are key to the development of effective antifibrotic strategies.

The vitamin D receptor (VDR) is a member of the nuclear hormone receptor (NHR) superfamily and is a key regulator of calcium homeostasis and skeletal health (Bouillon et al., 2008; Goltzman et al., 2004). The endogenous activators of this receptor are the biologically active form of vitamin D ($1,25(OH)_2D_3$) and bile acids such as lithocholic acid (LCA) and its derivatives (LCA-acetate, LCA-formate, 3-keto LCA) (Makishima et al., 2002; Nagpal et al., 2005). Interestingly, the closest structural and functional relatives of VDR within the NHR superfamily include farnesoid X receptor (FXR), constitutive androstane receptor (CAR), and pregnane X receptor (PXR), all of which are regulators of bile acid homeostasis and xenobiotic detoxification in the liver (Bookout et al., 2006; Bouillon et al., 2008). However, a physiological role for vitamin D in hepatic function has long been dismissed due to low levels of VDR expression in liver (Bookout et al., 2006; Han et al., 2010). Nonetheless, the finding of robust VDR expression in HSCs led us to consider it as a possible modulator of liver fibrosis (Gascon-Barré et al., 2003).

Here, we demonstrate that liver fibrosis in a standard mouse model of hepatic injury can be ameliorated by administration of the synthetic VDR agonist calcipotriol, which reduces both collagen deposition and fibrotic gene expression. We also show that *Vdr* knockout mice develop spontaneous liver fibrosis, proving a role for this receptor in normal liver homeostasis. Mechanistic studies revealed that activation of VDR signaling antagonizes a wide range of TGFβ/SMAD-dependent transcriptional responses on profibrotic genes in HSCs. Mapping of genome-wide binding sites of VDR and SMAD3 revealed overlapping DNA occupancy of these transcription factors on *cis*-regulatory elements of profibrotic genes. Interestingly, TGFβ/SMAD signaling enhanced the accessibility of liganded VDR with these genomic loci, which in turn antagonized recruitment of SMAD3. This dynamic VDR/SMAD genomic feedback circuit represents a previously unrecognized mechanism for regulating hepatic fibrogenesis.

RESULTS

VDR Prevents Liver Fibrosis

Consistent with previous results (Abramovitch et al., 2011; Gascon-Barré et al., 2003), we found that Vdr is expressed in HSCs but is not detectable in either whole liver or purified hepatocytes (Figures S1A–S1C available online). Moreover, the HSC-expressed VDR is fully functional as determined by ligand induction of CYP24A1 expression by either $1,25(OH)_2D_3$ or its low-calcemic analog, calcipotriol (Cal) (Nagpal et al., 2005) (Figure S2A), in both primary HSCs and LX-2 cells, a well-established TGFβ1-responsive human HSC cell line (Xu et al., 2005) (Figures S1D and S1E).

To address whether VDR signaling could suppress fibrotic gene expression and counteract hepatic fibrogenesis in vivo, liver fibrosis was induced by carbon tetrachloride (CCl_4), a widely used hepatotoxic agent, at a dose of 0.5 ml/kg administered by intraperitoneal (IP) injection three times per week in wild-type C57BL/6J mice. By 4 weeks, CCl_4-treated mice exhibited extensive liver bridging fibrosis with substantial collagen deposition, whereas CCl_4/calcipotriol-cotreated mice had a significant reduction in fibrosis as demonstrated by quantitation of Sirius red staining, hepatic hydroxyproline content, and histological fibrotic scoring (Figures 1A–1D). The serum calcium concentration was not significantly altered by calcipotriol treatment (Figure S2B). Examination of key fibrotic marker genes such as *Col1a1*, *Tgfb1*, and *Timp1* revealed between 50% and 70% downregulation by calcipotriol (Figures 1E–1G). Interestingly, when the mice were pretreated with calcipotriol for 5 weeks prior to CCl_4/calcipotriol-cotreatment, the fibrogenic response in liver was nearly completely abrogated (Figures S2C–S2F), suggesting that the VDR agonist possesses not only the ability to attenuate fibrosis but also the potential to proactively prevent liver fibrosis in vivo.

This led us to examine whether VDR deficiency could impact liver fibrogenesis. Indeed, 6-month-old $Vdr^{-/-}$ mice exhibited a spontaneous liver injury/fibrosis phenotype as demonstrated by increased collagen deposition, with two of four mice developing frank cirrhosis (Figure 1H, right/top) associated with hepatocyte necrosis and foci of necroinflammation surrounding portal tracts (Figure 1H, right/bottom, arrow). As there was some variability in the degree of liver fibrosis observed using Sirius red staining of liver sections, liver hydroxyproline content was

(E–G) qRT-PCR measurement of hepatic gene expression levels of Col1a1, Tgfβ1, and Timp1. Data represent the mean ±SEM. Asterisks denote statistically significant differences (Student's unpaired t test: **$p < 0.01$; ***$p < 0.001$).

(H) Sirius red (top) and H&E (bottom) stained liver sections from $Vdr^{+/+}$ (n = 3), $Vdr^{+/-}$ (n = 4), and $Vdr^{-/-}$ (n = 2 of 4) mice maintained on a calcium- and phosphate-supplemented rescue diet (2% calcium, 1.25% phosphorus, 20% lactose) for 6 months prior to sacrifice. Arrows indicate perisinusoidal fibrosis ($Vdr^{+/-}$ mice) and inflammatory cell infiltrate ($Vdr^{-/-}$ mice), respectively. Scale bar, 50 μm.

(I) Fibrosis quantified by hydroxyproline content and (J) Col1a1 mRNA expression using the two of four livers from $Vdr^{-/-}$ mice exhibiting the least fibrosis on Sirius red staining (refer to Results). Data represent the mean ±SEM. Asterisks denote statistically significant differences (Student's unpaired t test: *$p < 0.05$).

See also Figures S1 and S2.

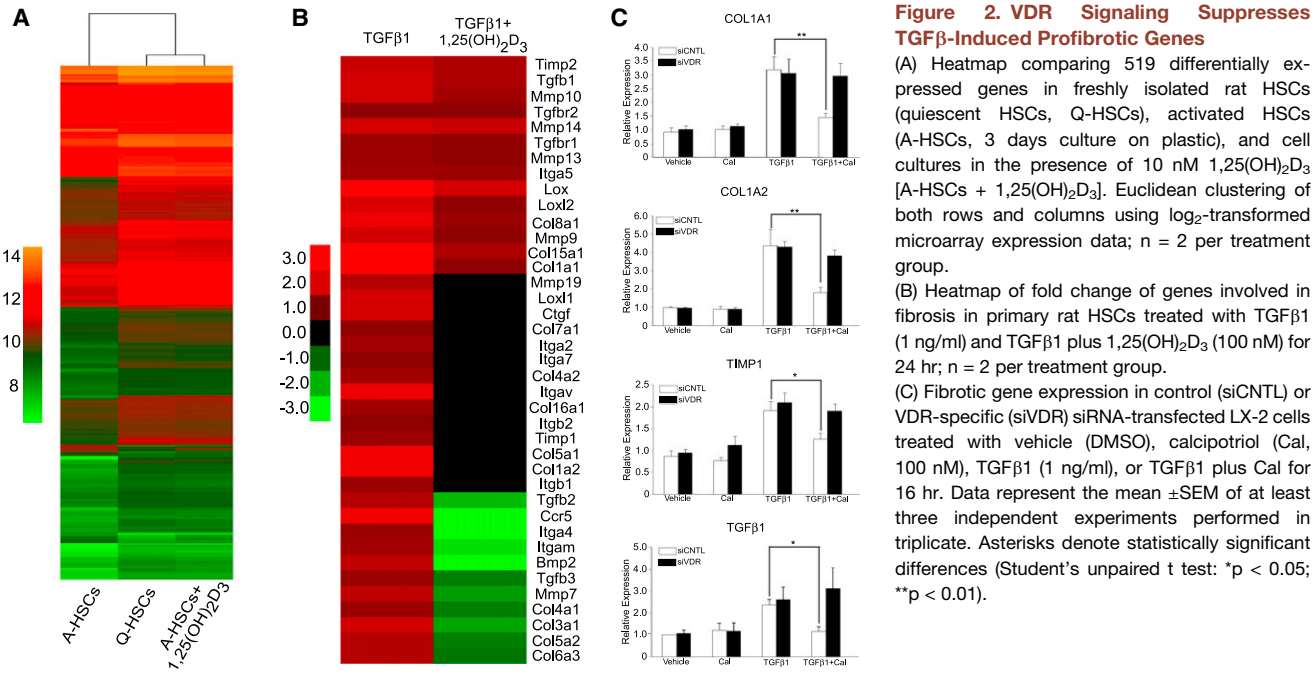

Figure 2. VDR Signaling Suppresses TGFβ-Induced Profibrotic Genes

(A) Heatmap comparing 519 differentially expressed genes in freshly isolated rat HSCs (quiescent HSCs, Q-HSCs), activated HSCs (A-HSCs, 3 days culture on plastic), and cell cultures in the presence of 10 nM $1,25(OH)_2D_3$ [A-HSCs + $1,25(OH)_2D_3$]. Euclidean clustering of both rows and columns using log_2-transformed microarray expression data; n = 2 per treatment group.

(B) Heatmap of fold change of genes involved in fibrosis in primary rat HSCs treated with TGFβ1 (1 ng/ml) and TGFβ1 plus $1,25(OH)_2D_3$ (100 nM) for 24 hr; n = 2 per treatment group.

(C) Fibrotic gene expression in control (siCNTL) or VDR-specific (siVDR) siRNA-transfected LX-2 cells treated with vehicle (DMSO), calcipotriol (Cal, 100 nM), TGFβ1 (1 ng/ml), or TGFβ1 plus Cal for 16 hr. Data represent the mean ±SEM of at least three independent experiments performed in triplicate. Asterisks denote statistically significant differences (Student's unpaired t test: *$p < 0.05$; **$p < 0.01$).

measured in the two $Vdr^{-/-}$ mice exhibiting the least fibrosis (noncirrhotic mice) and was still found to be significantly greater than that observed in either wild-type or $Vdr^{+/-}$ mice (Figure 1I). Moreover, $Vdr^{+/-}$ mice exhibited multiple foci of perisinusoidal fibrosis in the absence of an inflammatory response (Figure 1H, center/top, arrows), a pathology not observed in control wild-type mice maintained on an identical calcium- and phosphate-supplemented diet (Figure 1H, left). Histological findings were confirmed by quantitation of hepatic hydroxyproline content as well as examination of key fibrotic marker gene, *Col1a1* (Figures 1I and 1J). These data suggest that both *Vdr* alleles are required for the maintenance of normal liver architecture and that when completely abrogated, the result is loss of control of the local inflammatory response in addition to dysregulation of fibrogenesis.

VDR Signaling Suppresses TGFβ-Induced Profibrotic Genes

Expression profiling was used to explore the potential impact of VDR signaling in TGFβ1 and TGFβ1 plus $1,25(OH)_2D_3$-treated primary rat HSCs. Notably, $1,25(OH)_2D_3$ treatment attenuated the culture-induced activation of HSCs, such that the transcriptome of treated cells closely resembled that of freshly isolated quiescent cells (Figure 2A) and cotreatment of $1,25(OH)_2D_3$ together with TGFβ1 resulted in considerable repression of a large set of TGFβ1 induced genes (Table S1). Among these, we noted 39 genes central to hepatic fibrogenesis, including collagens (Bataller and Brenner, 2005; Tsukada et al., 2006), Tgf superfamily members (Inagaki and Okazaki, 2007), matrix metalloproteinase family members (Mmps) (Arthur, 2000; Han, 2006), tissue inhibitors of metalloproteinase (Timps) (Arthur, 2000; Yoshiji et al., 2002), integrins (Patsenker and Stickel, 2011), and lysyl oxidase family members (Barry-Hamilton et al., 2010; Kagan and Li, 2003; Vadasz et al., 2005) (Figure 2B).

Next, we confirmed that calcipotriol potently repressed fibrotic gene expression in both primary mouse HSCs and LX-2 cells, suggesting that the anti-TGFβ properties of VDR agonists are likely conserved across mammalian species (data not shown and Figure 2C). Finally, using RNA interference (RNAi) in LX-2 cells, we found that loss of VDR abolished calcipotriol-mediated repression of TGFβ1-induced gene expression (Figure 2C), collectively revealing that VDR regulates an anti-TGFβ/fibrotic network in vitro.

Defining VDR and SMAD3 Cistromes in HSCs

A major question raised by these observations was whether VDR was a direct or indirect regulator of the antifibrotic gene network. As SMAD2 and SMAD3 are required for TGFβ1-induced profibrotic gene expression in HSCs (Figure S3A) and VDR activation did not significantly affect TGFβ1-induced phosphorylation and subsequent nuclear translocation of SMAD3 (Figure S3B), we proposed a direct regulatory role for VDR. To explore this possibility, we analyzed the genome-wide binding sites of VDR and SMAD3 in LX-2 cells cultured with both calcipotriol and TGFβ1 using chromatin immunoprecipitation coupled with high-throughput deep sequencing (ChIP-seq). The resulting cistromes identified 24,984 VDR and 23,581 SMAD3 high-confidence binding sites (false discovery rate [FDR] < 0.0001) (Figures 3A and 3E). Consistent with the reported global binding pattern for other transcription factors (Barish et al., 2010; Biddie et al., 2011; Heinz et al., 2010; Trompouki et al., 2011), the majority of VDR- and SMAD3-binding sites localize to distant intergenic and intronic regions, whereas only 16%–21% are found at gene promoters (Figures 3A and 3E). From the list of VDR- and SMAD3-binding sites, we confirmed a number of previously

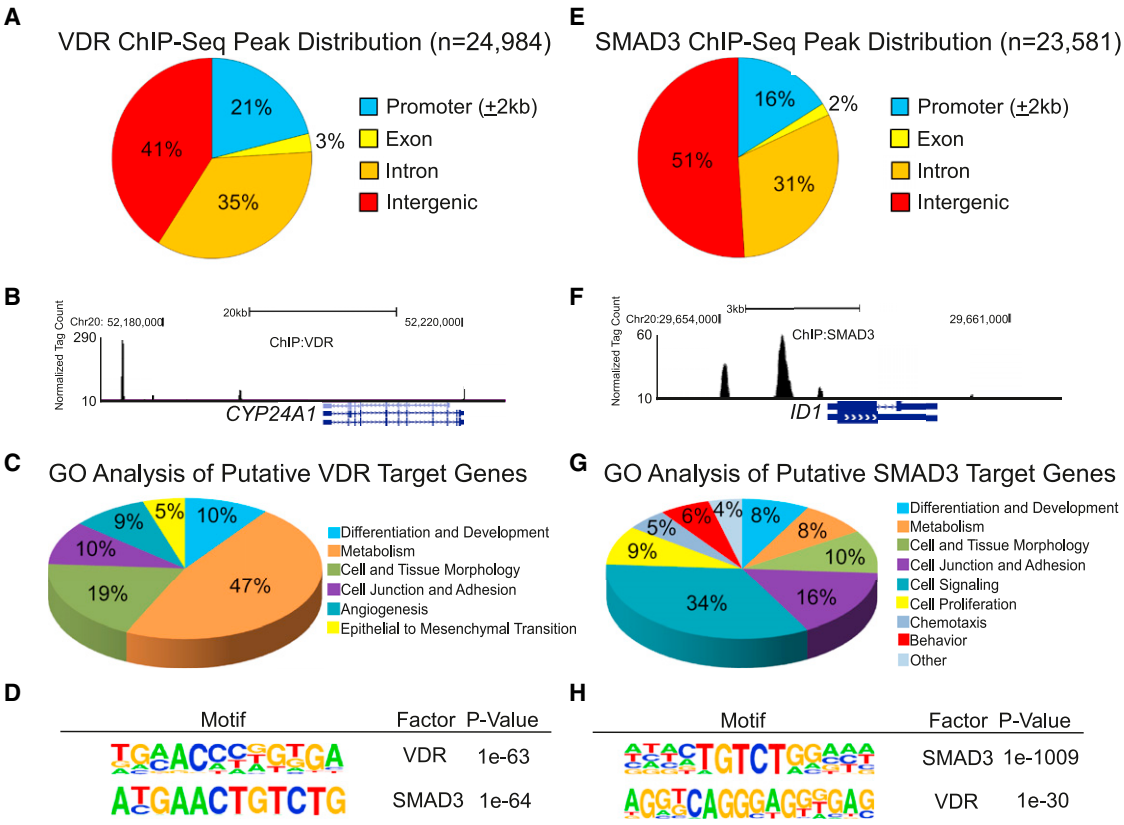

Figure 3. VDR and SMAD3 Cistromes in Hepatic Stellate Cells

(A and E) Pie charts illustrating genomic locations of VDR- and SMAD3-binding sites in treated LX-2 cells (100 nM calcipotriol and 1 ng/ml TGFβ1 for 4 hr following 16 hr 100 nM calcipotriol pretreatment; FDR < 0.0001). Promoter regions, <2 kb from the transcription start site; intergenic regions, not promoter, intron, or exon.

(B and F) Representative ChIP-seq reads for VDR and SMAD3 aligned to the CYP24A1 and ID1 genes, respectively.

(C and G) Gene ontology (GO) classification of genes annotated with VDR- and SMAD3-binding sites.

(D and H) De novo motif analysis performed on sequences located within 100 bp of VDR and SMAD3 peaks (FDR < 0.0001).

See also Figures S3 and S4.

characterized functional vitamin D response elements (VDRE) for known vitamin-D-inducible genes, such as *CYP24A1* (Figure 3B), *SPP1*, and *BGLAP* (Figures S4A and S4B), and SBE for TGFβ signaling target genes, including *ID1* (Figure 3F), *SMAD7*, and *TGFβI* (Figures S4C and S4D). Gene annotation analysis assigned peaks based on the proximity to the closest transcription start site and yielded 11,031 and 9,210 putative target genes within the individual VDR and SMAD3 cistromes, respectively. Gene ontology (GO) analysis of these annotated genes revealed that the most common classified functions for putative VDR and SMAD3 target genes were metabolism (47%) and cell signaling (34%) (Figures 3C and 3G).

Finally, we interrogated the most significantly enriched binding motifs for VDR and SMAD3. Among these sequence signatures, a direct hexamer repeat with a 3 bp spacer (DR3) consensus sequence was the most enriched motif at VDR sites, explaining 74% of VDR binding peaks (Figure 3D, top), while the consensus SBE sequence, a GTCT motif, accounted for 83% of SMAD3 binding peaks (Figure 3H, top). Interestingly, our analysis revealed that the GTCT and DR3-type motifs are also coenriched within nucleosomal distance at VDR- and SMAD3-binding sites, respectively, suggesting that VDR and SMAD3 communicate via intersecting cistromes (Figures 3D and 3H, bottom).

Antagonism of TGFβ Signaling via VDR/SMAD3 Genomic Crosstalk

To address this possibility, we used bioinformatic analysis to quantify the extent of cistrome intersection by calculating the number of sites bound by both VDR and SMAD3. A total of 10,436 genomic sites were co-occupied (Figure 4A), and the co-occupancy pattern is genome-wide as visualized by a heatmap quantifying VDR sites surrounding SMAD3 binding peaks (Figure 4B). If this genomic intersection mediates VDR/SMAD3 crosstalk, then VDR and SMAD3 could interact with their co-occupied sites simultaneously. Sequential ChIP (ChIP-re-ChIP) experiments confirmed that VDR and SMAD3 can, at least transiently, co-occupy the same genomic sites (Figure 4C).

Next, if anti-TGFβ signaling is mediated by a VDR/SMAD genomic intersection, then profibrotic genes in HSCs should be overrepresented in jointly bound regulatory elements. Indeed, GO analysis designating human phenotypes showed significant enrichment of "abnormal scarring" response (67%) for loci

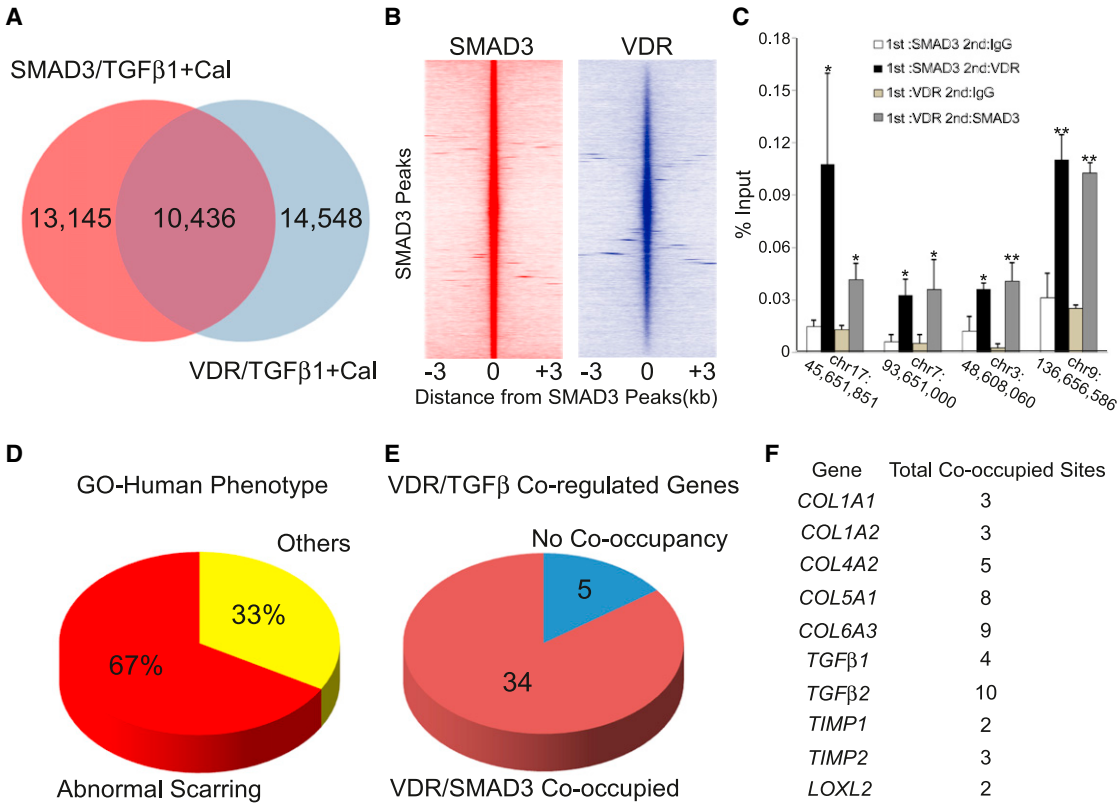

Figure 4. Antagonism of TGFβ Signaling via VDR/SMAD3 Genomic Crosstalk

(A) Venn diagram depicting overlap of VDR and SMAD3 genomic binding sites in LX-2 cells treated as in Figure 3.

(B) Intensity plots showing hierarchical clustering of ChIP-fragment densities as a function of distance from the center of statistically significant SMAD3 binding peaks (23,532 peaks; FDR = 0.0001). Intensity around position 0 of VDR (blue) indicates overlapping VDR/SMAD3 sites with SMAD3 (red) acting as a positive control.

(C) ChIP-re-ChIP of treated LX-2 cells analyzed by qPCR at VDR and SMAD3 cobound sites. Occupancy is expressed relative to input chromatin.

(D) Common human phenotypes enriched in genes co-occupied by VDR and SMAD3.

(E) The number of TGFβ1/VDR-coregulated profibrotic genes harboring genomic sites co-occupied by VDR and SMAD3.

(F) The number of VDR/SMAD3 co-occupied sites observed in profibrotic genes coregulated by TGFβ1 and VDR. LX-2 cells treated as in Figure 3. Data represent the mean ±SEM of at least three independent experiments performed in triplicate. Asterisks denote statistically significant differences (Student's t test: *$p < 0.05$; **$p < 0.01$).

See also Table S2 and Figure S5.

co-occupied by VDR and SMAD3 (Figure 4D), leading us to examine potential VDR/SMAD3 co-occupancy with the earlier identified 39 profibrotic genes (Figure 2B). Within this subset, 34 were found to contain VDR/SMAD3 co-occupied sites (Figure 4E). Furthermore, many of these genes were found to contain multiple VDR/SMAD3 co-occupied sites (Figure 4F; Table S2). Finally, we engineered luciferase reporter plasmids bearing VDR/SMAD3-cobound sites on the *COL1A1* gene and showed that these genomic elements could at least partially recapitulate the opposing actions of calcipotriol and TGFβ1, suggesting that these *cis*-elements function as enhancers of profibrotic gene expression (Figure S5A).

VDR/SMAD Genomic Antagonism

Informatic analysis of the spatial relationships between VDR and SMAD3 in co-occupied genomic regions confirmed that their respective response elements were colocalized within one nucleosomal window (≤200 base pairs) (Figure S5B), further supporting the possibility of genomic antagonism by proximal DNA binding (Barish et al., 2010; Hua et al., 2009).

The presence of VDR/SMAD genomic antagonism can be visualized by plotting the average ChIP-seq signal intensity of VDR and SMAD3 to the center of their co-occupied sites. This demonstrated that, in the presence of calcipotriol, TGFβ-induced recruitment of SMAD3 was globally compromised by ~1.5-fold, whereas binding of VDR to these sites was globally enhanced by nearly 10-fold (Figures 5A and 5B). In addition, the proposed genomic antagonism was illustrated by examining its impact along a profibrotic gene harboring VDR/SMAD co-occupied regulatory elements such as *COL1A1*. Visualization of sequencing tracks revealed that calcipotriol promoted VDR occupancy at all three major VDR/SMAD3-cobound sites on the *COL1A1* gene (Figure 5C, middle two tracks). In contrast, TGFβ-induced SMAD3 binding was typically diminished along

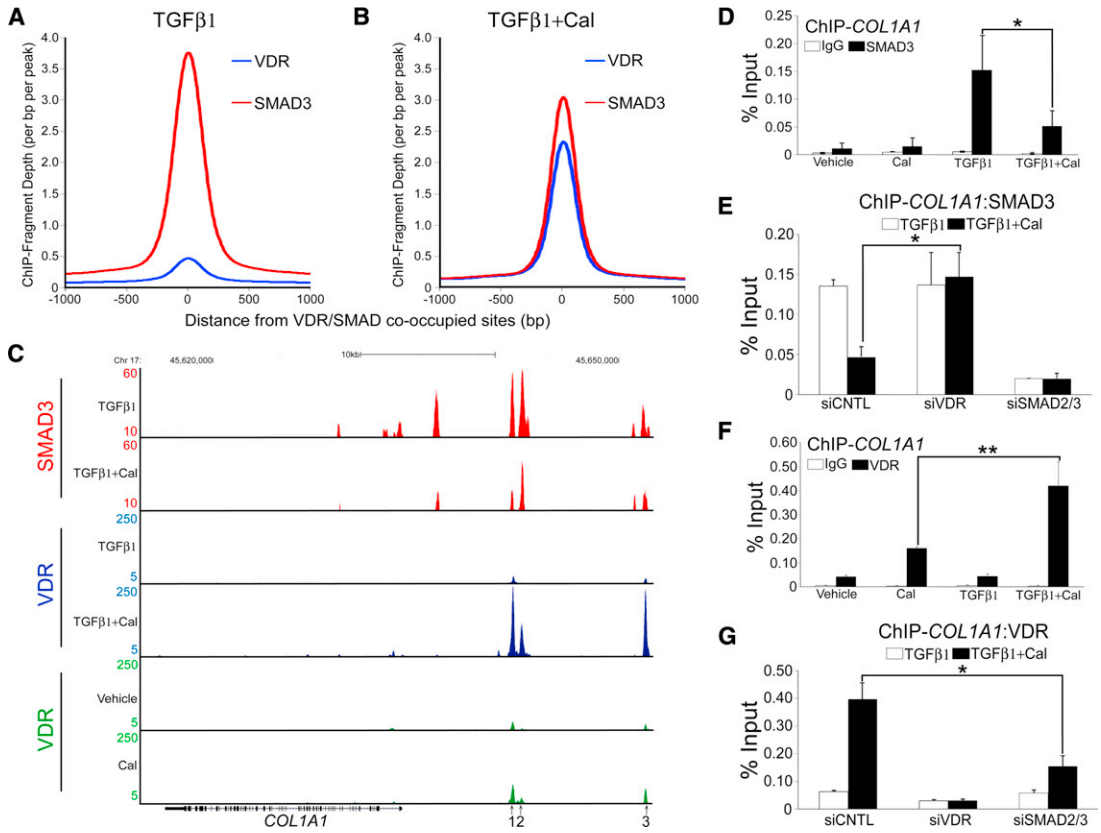

Figure 5. Genomic Antagonism between VDR and SMAD

(A and B) Plots of VDR and SMAD3 ChIP-seq signal intensity relative to the center of VDR/SMAD3 co-occupied sites in LX-2 cells (1 ng/ml TGFβ1 ± 100 nM calcipotriol for 4 hr).

(C) Representative ChIP-seq reads aligned to *COL1A1* for VDR and SMAD3 in treated LX-2 cells (vehicle [DMSO], 100 nM calcipotriol [Cal], 1 ng/ml TGFβ1, or TGFβ1 plus calcipotriol). The three co-occupied sites are designated as 1, 2, and 3.

(D and F) ChIP-qPCR at *COL1A1* regulatory region #1 cobound by VDR and SMAD3 in LX-2 cells treated as above.

(E and G) ChIP-qPCR at *COL1A1* regulatory region #1 of control (siCNTL), VDR-specific (siVDR), or SMAD3-specific (siSMAD3) siRNA-transfected LX-2 cells treated as above. Occupancy is expressed relative to input chromatin. Data represent the mean ±SEM of at least three independent experiments performed in triplicate. Asterisks denote statistically significant differences (Student's t test: $p < 0.05$; $^{**}p < 0.01$).

See also Figures S6 and S7.

the gene upon calcipotriol treatment (Figure 5C, top two tracks, and independently validated by ChIP quantitative PCR [ChIP-qPCR], Figures 5D and 5F). Similar loss of SMAD3 coupled with VDR recruitment was also observed at the regulatory regions of other profibrotic genes such as *COL1A2*, *TGFB1*, *TGFB2*, *TIMP1*, *TIMP2*, and *LOXL2* (Figures S6A–S6F). Furthermore, RNAi-mediated depletion of VDR and SMAD2/3 reversed the calcipotriol-dependent loss of SMAD3 recruitment and TGFβ1-induced VDR binding to co-occupied regulatory elements, respectively, demonstrating that VDR and SMADs are required to mediate this genomic antagonism (Figures 5E and 5G).

Since recruitment of histone-modifying cofactors such as CBP and p300 and hyperacetylation of histone H3 have been established as landmark events in the activation of TGFβ signaling (Massagué et al., 2005), we asked whether VDR/SMAD genomic antagonism could restrain TGFβ signaling by interfering with this epigenetic pathway. We therefore examined the status of histone H3 acetylation as well as recruitment of CBP and p300 to VDR/SMAD co-occupied sites in cells treated with either calcipotriol or TGFβ1 or both. ChIP-qPCR demonstrated that TGFβ1 induced recruitment of p300 and CBP and histone H3 hyperacetylation at the VDR/SMAD co-occupied regulatory region of *COL1A1*. This effect was lost in cells cotreated with calcipotriol and TGFβ1 (Figure S7A), suggesting that VDR/SMAD genomic antagonism limits TGFβ activation by compromising coactivator recruitment and histone hyperacetylation.

Ligand-dependent corepressor recruitment or "transrepression" has been proposed as the major mechanism for nuclear receptors such as PPARγ and LXR to negatively regulate inflammatory gene expression (Glass and Saijo, 2010). To test whether transrepression contributes to the antagonism, we examined potential induced recruitment of corepressors, including NCoR, SMRT, HDAC3, CoREST, LSD1, and G9a, to VDR/SMAD3 co-occupied regulatory regions of profibrotic genes, such as *COL1A1* and *COL1A2*, in response to calcipotriol and TGFβ1.

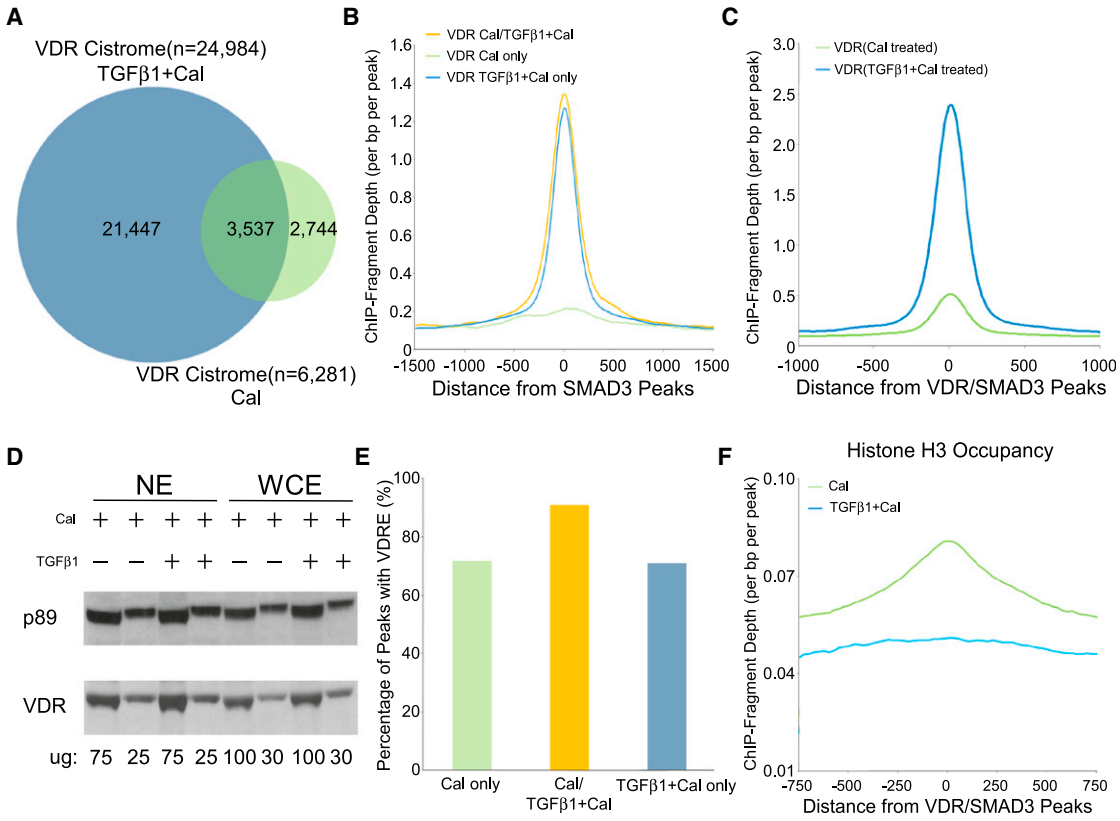

Figure 6. TGFβ Unmasks a Signal-Dependent VDR Cistrome

(A) Venn diagram displaying overlapping VDR cistromes in treated LX-2 cells (FDR < 0.0001).

(B) Plot of VDR ChIP-seq peak locations depicted in (A) categorized as VDR Cal/TGFβ1 plus Cal (3,537 overlapping), VDR Cal only (2,744 calcipotriol only), or VDR TGFβ1 plus Cal only (21,447 calcipotriol plus TGFβ1 only) relative to the center of SMAD3-binding sites in LX-2 cells.

(C) Plot of VDR ChIP-seq signal intensity relative to the center of VDR/SMAD3 co-occupied sites in LX-2 cells treated as indicated.

(D) Western blot for VDR in nuclear and whole-cell extracts (NE, WCE) from LX-2 cells treated as above. TFIIH (p89) was used as a loading control.

(E) The percentages of calcipotriol-only, calcipotriol plus TGFβ1-only, or calcipotriol/calcipotriol plus TGFβ1-overlapping VDR ChIP-seq peaks containing VDREs.

(F) Plot of histone H3 ChIP-seq signal intensity relative to the center of VDR/SMAD3 co-occupied sites in LX-2 cells treated as indicated.

See also Figure S6.

However, altered binding of these corepressors to these sites could not be detected (Figure S7B), suggesting that the loss of transcriptional activation complexes from these sites is not due to increased corepressor recruitment.

TGFβ Unmasks a Signal-Dependent VDR Cistrome

While establishing VDR/SMAD3 genomic antagonism, we noticed that TGFβ/SMAD signaling appears to enhance liganded VDR recruitment to the *cis*-regulatory regions of *COL1A1* (Figures 5F and 5G). To determine whether this effect is observed at other VDR-binding sites of profibrotic genes, we analyzed the VDR cistrome ± calcipotriol in the presence and absence of TGFβ1. Examination of binding data demonstrated that TGFβ1 promotes binding of liganded VDR, but not unliganded VDR, to *cis*-regulatory regions at all profibrotic genes (Figure 5B; Figures S6A–S6F, lower four tracks).

Next, we compared calcipotriol-induced VDR global binding patterns in the presence or absence of TGFβ1. While 6,281 binding sites comprise the de novo VDR cistrome in the absence of TGFβ1, a new cistrome composed of 24,984 sites was induced in the presence of TGFβ1 (Figure 6A). Interestingly, only 3,537 sites were shared by both cistromes, and 85% (21,447 sites) of the TGFβ-induced liganded VDR-binding sites were unique (Figure 6A), suggesting that TGFβ results in a dramatic shift of genome-wide binding locations of liganded VDR.

Comparative studies of the two VDR cistromes revealed that TGFβ1 plus calcipotriol sites (but not calcipotriol-only sites) were highly enriched at SMAD3-binding sites (Figure 6B). Moreover, binding of VDR to these genomic sites was enhanced by TGFβ signaling (Figure 6C), and this effect was not likely due to a change of VDR expression (Figure 6D). We next analyzed the DNA sequences of different subsets of VDR genomic loci and found more than 70% contain de novo VDR regulatory sites (Figure 6E), suggesting that VDR acts directly on the DNA, as opposed to SMAD-dependent tethering. Interestingly, we observed that TGFβ induced significant depletion of nucleosomes at VDR-SMAD3 cobound sites (Figure 6F), indicating that TGFβ-SMAD signaling may promote binding of VDR to its

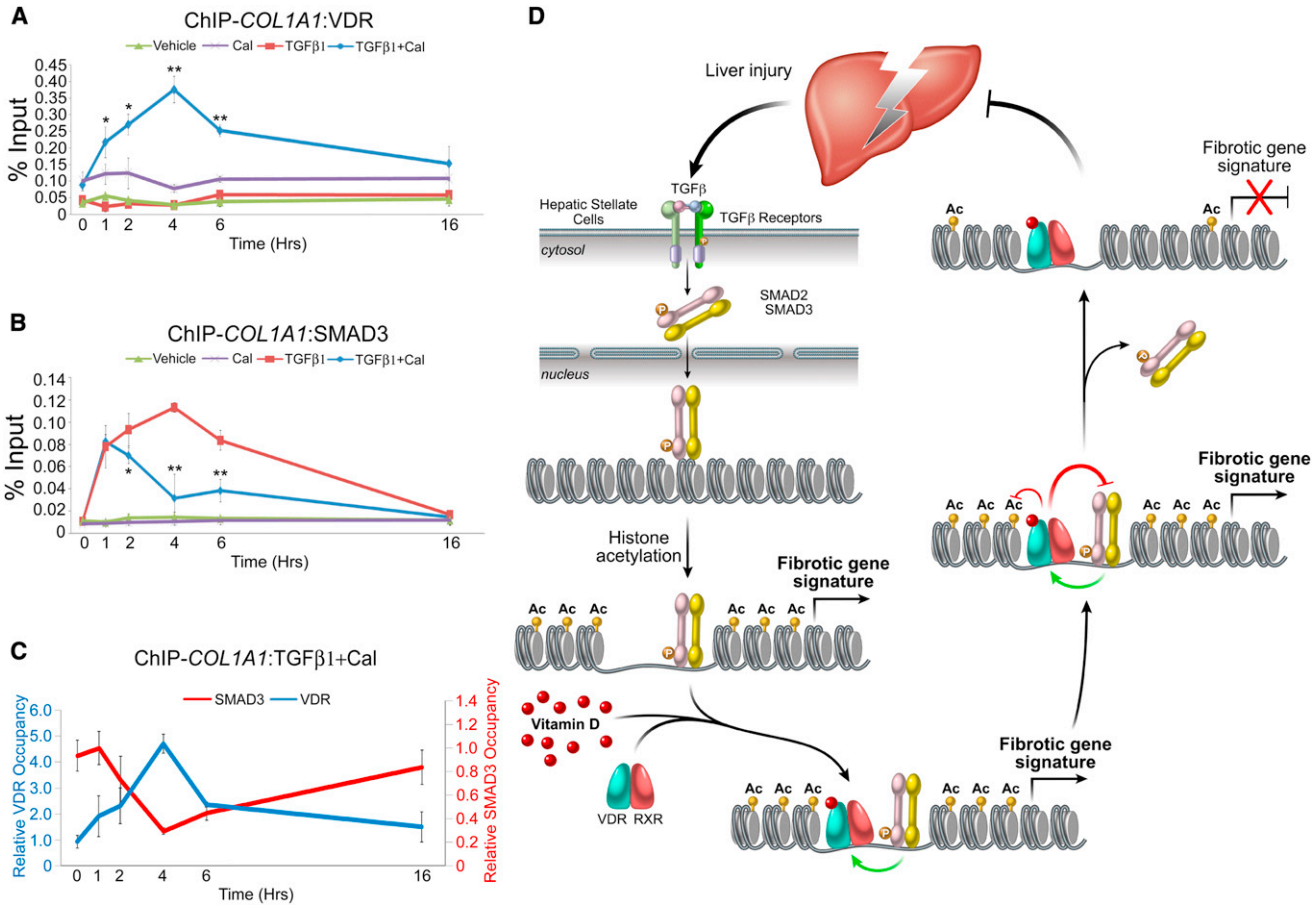

Figure 7. VDR/SMAD Genomic Circuit

(A and B) Time course of VDR and SMAD3 binding at the *COL1A1* regulatory region #1 in treated LX-2 cells (vehicle [DMSO], 100 nM calcipotriol, 1 ng/ml TGFβ1, 1 ng/ml TGFβ1 plus 100 nM calcipotriol) determined by ChIP-qPCR. LX-2 cells were pretreated with calcipotriol (100 nM) for 16 hr prior to time course assay and occupancy is expressed relative to input chromatin. Data represent the mean ±SEM of at least three independent experiments performed in triplicate. Asterisks denote statistically significant differences compared to calcipotriol-induced VDR occupancy or TGFβ1-induced SMAD3 occupancy of corresponding time point (Student's unpaired t test: *$p < 0.05$; *$p < 0.01$).

(C) Time course of TGFβ1 plus calcipotriol-induced VDR and SMAD3 binding, normalized to calcipotriol alone or TGFβ1 alone, respectively. Data represent the mean ±SEM of at least three independent experiments performed in triplicate.

(D) Model depicting proposed VDR/SMAD genomic circuit controlling profibrogenic responses in HSCs.

adjacent sites by potentiating local chromatin remodeling and resultant accessibility.

The Genomic Circuit between VDR and SMAD

Our findings suggest a dynamic relationship between VDR and TGFβ/SMAD signaling; perhaps TGFβ induction of SMAD binding to chromatin creates a new genomic landscape that now becomes accessible to liganded VDR, which could enable temporally delayed SMAD repression. To explore this spatiotemporal relationship, we determined the kinetics of SMAD3 and VDR recruitment to co-occupied *cis*-regulatory elements of fibrotic genes (such as *COL1A1*) in the presence of either calcipotriol or TGFβ1 or both. Specifically, ChIP-qPCR was employed to monitor binding of VDR and SMAD3 to the *cis*-regulatory region of *COL1A1* at multiple time points (0, 1, 2, 4, 6, and 16 hr). Notably, binding of both liganded VDR and SMAD3 to this site was maximally promoted by TGFβ1 after 4 hr of treatment, followed by a gradual decrease to basal levels after 16 hr (Figures 7A ad 7B), confirming the role of TGFβ1 in facilitating recruitment of VDR to chromatin. Interestingly, the binding curve of SMAD3 upon TGFβ1 stimulation was dramatically shifted by the presence of calcipotriol, with the maximum binding of SMAD3 observed just 1 hr post-TGFβ1 treatment. After 4 hr, SMAD3 recruitment was significantly reduced by 70% (Figure 7B). Furthermore, normalization of VDR and SMAD3 binding in the presence of both calcipotriol and TGFβ1 to their basal levels revealed that the occupancy of VDR and SMAD3 were inversely correlated (Figure 7C), suggesting TGFβ-induced chromatin accessibility produces a genomic architecture that facilitates VDR to reverse SMAD activation. Together, this VDR/SMAD genomic circuit provides a chromatin-based mechanism for VDR to block fibrosis by antagonizing TGFβ signaling in HSCs.

DISCUSSION

The establishment of HSCs as the primary effector cell for the deposition of ECM in normal and fibrotic liver in the early 1990s was a milestone discovery in understanding the pathogenesis of hepatic fibrosis (Friedman, 1993). Since then, a wide spectrum of cellular signaling molecules, hormones, cell membrane receptors, and transcription factors in HSCs have been investigated and found to promote hepatic fibrogenesis (Hernandez-Gea and Friedman, 2011). However, the factors and signaling cascades that actively prevent this pathological process are poorly understood. Here, we demonstrate that pharmacological activation of VDR attenuates the progression of liver fibrosis in an experimental animal model while genetic abrogation of VDR expression results in the spontaneous development of liver fibrosis, thus implicating VDR in an endocrine checkpoint that negatively modulates the wound-healing response in liver. Mechanistically, we delineate a previously unrecognized and temporally controlled genomic circuit composed of the opposing action of VDR and SMAD transcription factors that is able to restrain the intensity of the fibrogenic response in HSCs and govern fibrogenesis in liver. Specifically, in response to liver injury, HSC activation by TGFβ1 induces profibrotic gene expression via SMAD translocation to the nucleus and chromatin remodeling. By increasing accessibility to adjacent VDREs, SMAD activation facilitates VDR recruitment to previously cryptic genomic sites. Liganded VDR subsequently antagonizes SMAD residency on chromatin and compromises acetylation of histone H3 to ultimately suppress profibrotic gene expression (Figure 7D). Notably, the proximal location of nearly 10,500 TGFβ1-induced SMAD- and VDR-binding sites identifies a global chromatin architecture and suggests that the integrated VDR/SMAD genomic circuit functions as a master regulator of the hepatic fibrotic response.

The identification of a chromatin basis for inhibiting TGFβ signaling places a direct focus on SMAD-dependent transcription as a regulatory target. This is relevant because TGFβ/SMAD signaling plays an essential role in almost every aspect of metazoan biology, and its dysregulation can result in a diversity of human diseases ranging from autoimmunity to fibrosis and cancer (Hernandez-Gea and Friedman, 2011; Li and Flavell, 2008; Massagué, 2008). Our finding of genomic antagonism between VDR and SMAD not only establishes VDR as the first DNA binding transcription factor that attenuates TGFβ/SMAD signaling at a chromatin interface, but also adds specificity (a cistromic layer) for the more general concept of "transcriptional crosstalk."

The observation that TGFβ-SMAD activation enables subsequent recruitment of ligand-bound VDR to repress SMAD targets reveals a means by which two endogenous signaling pathways can cross-regulate each other's activity. Thus, this genomic relay allows positive activation by SMAD to be subsequently inhibited by VDR and thus constitutes a self-adjusting genomic circuit, which is highly distinguishable from the previously reported genomic crosstalk between transcription factors in a mutually exclusive manner (Barish et al., 2010; Hua et al., 2009). It seems logical that this circuit may confer on HSCs the ability to orchestrate ECM synthesis in both the normal and fibrotic liver.

In addition to the TGFβ/SMAD pathway, fibrosis is almost always preceded by persistent inflammation clinically (Hernandez-Gea and Friedman, 2011; Lee and Friedman, 2011). Hence, a broader anti-inflammatory role for VDR signaling might conceivably contribute to its antifibrotic property in the liver. In this regard, VDR has been documented for its expression in several cell types central to the inflammatory response (Barish et al., 2005; Griffin et al., 2001; von Essen et al., 2010), and both vitamin D deficiency and polymorphisms of VDR itself as well as genes involved in vitamin D metabolism have been linked to both the risk and severity of inflammatory diseases (Agmon-Levin et al., 2012; Janssens et al., 2011; Munger et al., 2006; Ramagopalan et al., 2011). However, the role of VDR signaling's anti-inflammatory action in the context of hepatic fibrogenesis is far less clear. On one hand, the dysregulated inflammatory response coupled with the spontaneous development of liver fibrosis in $Vdr^{-/-}$ mice suggests that VDR signaling might control hepatic fibrogenesis through an anti-inflammatory mechanism (Figure 1H, right). On the other hand, this notion is blunted by the modest perisinusoidal liver fibrosis phenotype without any inflammatory response found in $Vdr^{+/-}$ mice (Figure 1H, center). Furthermore, the causable relationship between inflammation and fibrosis remains to be fully established and the major profibrogenic role of inflammation during hepatic fibrogenesis appears to be to sensitize HSCs for TGFβ/SMAD activation (Seki et al., 2007; Seki and Schnabl, 2012). It is therefore unlikely that the anti-inflammatory property of VDR signaling plays a major role in its antifibrotic function.

Our studies further serve to clarify an unappreciated function of VDR signaling in liver pathophysiology. Due to its exceptionally low expression, VDR has received much less attention than its highly expressed cognate clade members that include FXR, PXR, and CAR that impact nearly every aspect of hepatic function including lipid and glucose metabolism, drug disposition, cholesterol efflux, and bile acid homeostasis (Bookout et al., 2006; Chawla et al., 2001). However, recent studies showing that low vitamin D levels are linked to increased hepatic fibrosis in patients with chronic liver disease (Abramovitch et al., 2011; Lim and Chalasani, 2012; Petta et al., 2010; Terrier et al., 2011) and that vitamin D can inhibit liver fibrosis in rats (Abramovitch et al., 2011) suggest a potential physiologic role for hepatic VDR. However, whether and how VDR directly or indirectly regulates hepatic fibrogenesis remained unresolved. Our findings that VDR promotes HSC quiescence and controls TGFβ signaling identify a new mechanism through which vitamin D can exert its antifibrotic effects. It is noteworthy that our delineation of a VDR signaling pathway to inhibit fibrosis is also consistent with recent studies suggesting that a polymorphism in VDR is correlated with increased progression of liver fibrosis and evolution of cirrhosis (Baur et al., 2012; Tanaka et al., 2009).

Up to 45% of deaths in the developed world can be attributed to fibrotic diseases, yet few antifibrotic drugs are currently approved for clinical use (Wynn, 2008). Though therapies designed to neutralize TGFβ show broad antifibrotic activity (Rosenbloom et al., 2010), the benefits are compromised by unnecessarily blocking TGFβ in nondiseased tissue. Our discovery of the VDR/SMAD genomic circuit illuminates a potentially safer

antifibrotic strategy by restricting TGFβ inhibition to VDR-positive cells instead of perturbing signaling body-wide.

In summary, our work describes an intersecting genomic circuit comprising VDR and SMAD transcription factors that governs hepatic fibrogenesis. This finding significantly extends our understanding of how two distinct signal-dependent transcription factors interact with each other to establish cell identity and function. Through the use of genetic and inducible models, we provide new insight into how global programs responding to TGFβ1 signaling are established and regulated. Furthermore, these studies establish VDR as a potential drug target to treat liver fibrosis and provide a new paradigm of VDR-dependent gene expression regulation. Given the ubiquitous expression patterns of VDR and TGFβ, the VDR/SMAD genomic circuit is likely to be applicable to many other cell types and may impact the pathogenesis of a wide range of human diseases.

EXPERIMENTAL PROCEDURES

All animal experiments were performed in specific pathogen-free facilities at the Salk Institute following the Institutional Animal Care and Use Committee's guidelines.

Primary HSCs Isolation and Culture

HSCs were isolated from 10-week-old male C57BL/6J mice and Wistar rats by in situ pronase, collagenase perfusion, and single-step Histogenz gradient as previously reported (Hendriks et al., 1985; Knook et al., 1982). Isolated HSCs were cultured in Dulbecco's modified Eagle's medium (Mediatech) containing 20% fetal bovine serum (Hyclone) on six-well plates for 40 hr prior to end-point assays.

Immunoprecipitation and Western Blot

The whole-cell lysates were obtained through RIPA buffer lysis while isolation of nuclear extract was performed as previously reported (Ding et al., 2008). Total SMAD3 was immunoprecipitated in nuclear extracts from LX-2 cells using anti-SMAD2/3 antibody (Santa Cruz, sc-133098) followed by SDS-PAGE and western blot detection by anti-SMAD3 (Cell Signaling, 9523) and anti-pSMAD3 (Cell Signaling, 9520) specific antibodies.

Cell Culture, Luciferase Assay, and qRT-PCR

LX-2 cells (a generous gift from Professor Scott Friedman, Mount Sinai School of Medicine, New York, NY) were cultured as described previously (Xu et al., 2005). TGFβ1 (R&D Systems), $1,25(OH)_2D_3$, and calcipotriol (Tocris) were used at concentrations of 1 ng/ml, 100 nM, and 100 nM, respectively, except when otherwise indicated. For luciferase assays, DNA transfections were performed using Fugene 6 (Roche) following the manufacturer's instructions. Twenty-four hours following DNA transfections, cells were treated with vehicle, calcipotriol, or TGFβ1 or both for another 24 hr prior to luciferase/β-galactosidase assays (Promega). For quantitative RT-PCR (qRT-PCR), total RNA was purified following TRIzol extraction and treated with DNaseI (Life Technologies). Complementary DNA synthesis was carried out with iScript RT Supermix (Bio-Rad). Quantitative PCR was performed in technical triplicates using SYBR Green reagent (Bio-Rad). The relative standard curve method was used for quantitation (Bio-Rad). Expression levels were calculated by normalization to either Gapdh (mouse) or U36B4 (human) quantities. The sequences of primers are listed in Table S3.

Transfection of siRNAs

Transfection was carried out at a concentration of 20 nM of indicated small interfering RNAs (siRNAs) (in the case of SMAD2/3, 10 nM of each siRNA was combined for transfection) using RNAiMax transfection reagent (Life Technologies). Transfected cells were cultured without perturbation for at least 48 hr prior to terminal assays.

CCl_4 Model of Liver Injury and Fibrosis

Eight-week-old male C57BL/6J mice were IP injected with 0.5 ml/kg body weight CCl_4 (1:50 v/v in corn oil from Sigma) or vehicle (DMSO in corn oil) three times a week for 4 weeks. Calcipotriol (20 μg/kg body weight) was administered by oral gavage five times a week, commencing 20 days after the first dose of CCl_4. The animals were terminated 72 hr after the final CCl_4 injection, and whole livers and serum were collected for histological, cytological, biochemical, and molecular analyses.

Vdr Knockout Mice

C57BL/6J mice heterozygous for targeted ablation of *Vdr* (Li et al., 1997) were obtained from The Jackson Laboratory (stock number 006133). Wild-type controls, $Vdr^{+/-}$, and $Vdr^{-/-}$ mice were maintained on a $Vdr^{-/-}$ rescue diet (Amling et al., 1999) containing 21% calcium, 0.67% phosphorus, and 20% lactose supplemented with 4.4 U vitamin D per gram diet for 6 months prior to sacrifice. Livers were collected for analysis as above.

Fibrotic Score and Quantification of Hepatic Collagen and Hydroxyproline Content

Sections (5 μm) of formalin-fixed liver were stained following standard hematoxylin and eosin and Sirius red methods and reviewed by a pathologist who was blinded to the experimental conditions. Fibrosis was scored using the Ishak modified histological activity index (HAI) scoring system. Fibrosis was also quantified using Image J software on ten noncontiguous Sirius-red-stained sections. All images were obtained using a high-resolution Leica DFC420 digital camera mounted on an Olympus microscope equipped with ×4/0.13, ×10/0.30, ×20/0.50, and ×40/0.75 UplanFL N plan objective lenses and processed with the Leica Application Suite. Hepatic hydroxyproline content was measured using a commercial colorimetric assay from Biovision (K555-100).

ChIP and ChIP-Re-ChIP

LX-2 cells were pretreated with calcipotriol (100 nM) for 16 hr followed by incubation of calcipotriol (100 nM) or TGFβ1 (1 ng/ml) or both for an additional 4 hr. Cells were then harvested for the ChIP assay. The experimental procedure for ChIP was as previously described (Barish et al., 2010). Briefly, after fixation, nuclei from LX-2 cells were isolated, lysed, and sheared with a Diagenode Bioruptor to yield DNA fragment sizes of 200–1,000 bp followed by immunoprecipitation using the following antibodies: normal rabbit immunoglobulin G (Santa Cruz, sc-2027), VDR (Santa Cruz, sc-1008), SMAD3 (Abcam, ab28379), and histone H3 (Abcam, ab1791). For ChIP-re-ChIP, after the first ChIP, the immunoprecipitated DNA-protein complex was eluted from beads using 10 mM dithiothreitol and diluted 100-fold, followed by the second ChIP.

ChIP-Seq Data Analysis

The procedure was as previously described (Barish et al., 2010). Briefly, short DNA reads were aligned against the human hg18 reference genome (NCBI Build 36.1) using the Illumina Pipeline Suite v1.7. Reads were aligned using the Bowtie aligner, allowing up to two mismatches in the read. Only tags that map uniquely to the genome were considered for further analysis. Subsequent peak calling and motif analysis were conducted using HOMER, a software suite for ChIP-seq analysis. The methods for HOMER, which are described below, have been implemented and are freely available at http://biowhat.ucsd.edu/homer/ (Heinz et al., 2010). One tag from each unique position was considered to eliminate peaks resulting from clonal amplification of fragments during the ChIP-seq protocol. Peaks were identified by searching for clusters of tags within a sliding 200 bp window, requiring adjacent clusters to be at least 1 kb away from each other. The threshold for the number of tags that determine a valid peak was selected for an FDR < 0.0001, as empirically determined by repeating the peak finding procedure using randomized tag positions. Peaks are required to have at least 4-fold more tags (normalized to total count) than input or immunoglobulin G control samples and 4-fold more tags relative to the local background region (10 kb) to avoid identifying regions with genomic duplications or nonlocalized binding. Peaks are annotated to gene products by identifying the nearest RefSeq transcriptional start site. Visualization of ChIP-seq results was achieved by uploading custom

tracks onto the University of California, Santa Cruz genome browser. Human phenotype analysis was performed using GREAT (genomic regions enrichment of annotations tool) at http://great.stanford.edu/.

Microarray Data Analysis

Total RNA from primary rat or mouse HSCs was isolated using the RNeasy mini kit (QIAGEN) according to standard protocols. RNA integrity and quality was assessed using the Agilent Bioanalyzer and prepared for hybridization to Illumina rat or mouse gene expression arrays according to standard Illumina protocols. Feature extraction was performed using the Illumina GenomeStudio software. Normalization and identification of differentially expressed genes from biological duplicates was performed using VAMPIRE at http://sasquatch.ucsd.edu/vampire/.

ACCESSION NUMBERS

The Gene Expression Omnibus accession number for the full data sets (ChIP-seq and microarray) is GSE41580.

SUPPLEMENTAL INFORMATION

Supplemental Information includes seven figures and three tables and can be found with this article online at http://dx.doi.org/10.1016/j.cell.2013.03.028.

ACKNOWLEDGMENTS

We thank C. Brondos and E. Ong for administrative assistance, J. Nery for assistance with DNA sequencing, C. Benner for assistance with HOMER software, and H. Juguilon and J. Alvarez for technical assistance. N.D. was supported by a postdoctoral fellowship from Genentech Foundation. G.D.B. was supported by grant K08HL092298. This work was funded by grants from the National Institutes of Health (DK057978, HL105278, DK090962, HL088093, ES010337, and CA014195) and National Health and Medical Research Council of Australia project grants 512354 and 632886 (to C.L. and M.D.), as well as by the Helmsley Charitable Trust, Samuel Waxman Cancer Research Foundation, and Ipsen/Biomeasure. R.M.E. and M.D. are supported in part by a Stand Up to Cancer Dream Team translational cancer research grant, a Program of the Entertainment Industry Foundation (SU2C-AACR-DT0509). R.M.E is an investigator of the Howard Hughes Medical Institute and March of Dimes chair in molecular and developmental biology at the Salk Institute.

Received: October 12, 2012
Revised: January 14, 2013
Accepted: March 11, 2013
Published: April 25, 2013

REFERENCES

Abramovitch, S., Dahan-Bachar, L., Sharvit, E., Weisman, Y., Ben Tov, A., Brazowski, E., and Reif, S. (2011). Vitamin D inhibits proliferation and profibrotic marker expression in hepatic stellate cells and decreases thioacetamide-induced liver fibrosis in rats. Gut *60*, 1728–1737.

Agmon-Levin, N., Theodor, E., Segal, R.M., and Shoenfeld, Y. (2012). Vitamin D in Systemic and Organ-Specific Autoimmune Diseases. Clin. Rev. Allergy Immunol. *2012*, 14.

Amling, M., Priemel, M., Holzmann, T., Chapin, K., Rueger, J.M., Baron, R., and Demay, M.B. (1999). Rescue of the skeletal phenotype of vitamin D receptor-ablated mice in the setting of normal mineral ion homeostasis: formal histomorphometric and biomechanical analyses. Endocrinology *140*, 4982–4987.

Arthur, M.J. (2000). Fibrogenesis II. Metalloproteinases and their inhibitors in liver fibrosis. Am. J. Physiol. Gastrointest. Liver Physiol. *279*, G245–G249.

Barish, G.D., Downes, M., Alaynick, W.A., Yu, R.T., Ocampo, C.B., Bookout, A.L., Mangelsdorf, D.J., and Evans, R.M. (2005). A Nuclear Receptor Atlas: macrophage activation. Mol. Endocrinol. *19*, 2466–2477.

Barish, G.D., Yu, R.T., Karunasiri, M., Ocampo, C.B., Dixon, J., Benner, C., Dent, A.L., Tangirala, R.K., and Evans, R.M. (2010). Bcl-6 and NF-kappaB cistromes mediate opposing regulation of the innate immune response. Genes Dev. *24*, 2760–2765.

Barry-Hamilton, V., Spangler, R., Marshall, D., McCauley, S., Rodriguez, H.M., Oyasu, M., Mikels, A., Vaysberg, M., Ghermazien, H., Wai, C., et al. (2010). Allosteric inhibition of lysyl oxidase-like-2 impedes the development of a pathologic microenvironment. Nat. Med. *16*, 1009–1017.

Bataller, R., and Brenner, D.A. (2005). Liver fibrosis. J. Clin. Invest. *115*, 209–218.

Baur, K., Mertens, J.C., Schmitt, J., Iwata, R., Stieger, B., Eloranta, J.J., Frei, P., Stickel, F., Dill, M.T., Seifert, B., et al. (2012). Combined effect of 25-OH vitamin D plasma levels and genetic Vitamin D Receptor (NR 1I1) variants on fibrosis progression rate in HCV patients. Liver Int. *32*, 635–643.

Biddie, S.C., John, S., Sabo, P.J., Thurman, R.E., Johnson, T.A., Schiltz, R.L., Miranda, T.B., Sung, M.H., Trump, S., Lightman, S.L., et al. (2011). Transcription factor AP1 potentiates chromatin accessibility and glucocorticoid receptor binding. Mol. Cell *43*, 145–155.

Bookout, A.L., Jeong, Y., Downes, M., Yu, R.T., Evans, R.M., and Mangelsdorf, D.J. (2006). Anatomical profiling of nuclear receptor expression reveals a hierarchical transcriptional network. Cell *126*, 789–799.

Bouillon, R., Carmeliet, G., Verlinden, L., van Etten, E., Verstuyf, A., Luderer, H.F., Lieben, L., Mathieu, C., and Demay, M. (2008). Vitamin D and human health: lessons from vitamin D receptor null mice. Endocr. Rev. *29*, 726–776.

Bouwens, L., De Bleser, P., Vanderkerken, K., Geerts, B., and Wisse, E. (1992). Liver cell heterogeneity: functions of non-parenchymal cells. Enzyme *46*, 155–168.

Breitkopf, K., Godoy, P., Ciuclan, L., Singer, M.V., and Dooley, S. (2006). TGF-beta/Smad signaling in the injured liver. Z. Gastroenterol. *44*, 57–66.

Chawla, A., Repa, J.J., Evans, R.M., and Mangelsdorf, D.J. (2001). Nuclear receptors and lipid physiology: opening the X-files. Science *294*, 1866–1870.

Cohen-Naftaly, M., and Friedman, S.L. (2011). Current status of novel antifibrotic therapies in patients with chronic liver disease. Therap. Adv. Gastroenterol. *4*, 391–417.

Ding, N., Zhou, H., Esteve, P.O., Chin, H.G., Kim, S., Xu, X., Joseph, S.M., Friez, M.J., Schwartz, C.E., Pradhan, S., and Boyer, T.G. (2008). Mediator links epigenetic silencing of neuronal gene expression with x-linked mental retardation. Mol. Cell *31*, 347–359.

Feng, X.H., and Derynck, R. (2005). Specificity and versatility in tgf-beta signaling through Smads. Annu. Rev. Cell Dev. Biol. *21*, 659–693.

Friedman, S.L. (1993). Seminars in medicine of the Beth Israel Hospital, Boston. The cellular basis of hepatic fibrosis. Mechanisms and treatment strategies. N. Engl. J. Med. *328*, 1828–1835.

Friedman, S.L. (1999). Evaluation of fibrosis and hepatitis C. Am. J. Med. *107*(6B), 27S–30S.

Friedman, S.L. (2003). Liver fibrosis — from bench to bedside. J. Hepatol. *38*(*Suppl 1*), S38–S53.

Friedman, S.L. (2008). Hepatic stellate cells: protean, multifunctional, and enigmatic cells of the liver. Physiol. Rev. *88*, 125–172.

Friedman, S.L., and Bansal, M.B. (2006). Reversal of hepatic fibrosis — fact or fantasy? Hepatology *43*(2, Suppl 1), S82–S88.

Friedman, S.L., Roll, F.J., Boyles, J., and Bissell, D.M. (1985). Hepatic lipocytes: the principal collagen-producing cells of normal rat liver. Proc. Natl. Acad. Sci. USA *82*, 8681–8685.

Gascon-Barré, M., Demers, C., Mirshahi, A., Néron, S., Zalzal, S., and Nanci, A. (2003). The normal liver harbors the vitamin D nuclear receptor in nonparenchymal and biliary epithelial cells. Hepatology *37*, 1034–1042.

Geerts, A. (2001). History, heterogeneity, developmental biology, and functions of quiescent hepatic stellate cells. Semin. Liver Dis. *21*, 311–335.

Glass, C.K., and Saijo, K. (2010). Nuclear receptor transrepression pathways that regulate inflammation in macrophages and T cells. Nat. Rev. Immunol. *10*, 365–376.

Goltzman, D., Miao, D., Panda, D.K., and Hendy, G.N. (2004). Effects of calcium and of the Vitamin D system on skeletal and calcium homeostasis: lessons from genetic models. J. Steroid Biochem. Mol. Biol. *89-90*, 485–489.

Griffin, M.D., Lutz, W., Phan, V.A., Bachman, L.A., McKean, D.J., and Kumar, R. (2001). Dendritic cell modulation by 1alpha,25 dihydroxyvitamin D3 and its analogs: a vitamin D receptor-dependent pathway that promotes a persistent state of immaturity in vitro and in vivo. Proc. Natl. Acad. Sci. USA *98*, 6800–6805.

Han, S., Li, T., Ellis, E., Strom, S., and Chiang, J.Y. (2010). A novel bile acid-activated vitamin D receptor signaling in human hepatocytes. Mol. Endocrinol. *24*, 1151–1164.

Han, Y.P. (2006). Matrix metalloproteinases, the pros and cons, in liver fibrosis. J. Gastroenterol. Hepatol. *21*(*Suppl 3*), S88–S91.

Heinz, S., Benner, C., Spann, N., Bertolino, E., Lin, Y.C., Laslo, P., Cheng, J.X., Murre, C., Singh, H., and Glass, C.K. (2010). Simple combinations of lineage-determining transcription factors prime cis-regulatory elements required for macrophage and B cell identities. Mol. Cell *38*, 576–589.

Hendriks, H.F., Verhoofstad, W.A., Brouwer, A., de Leeuw, A.M., and Knook, D.L. (1985). Perisinusoidal fat-storing cells are the main vitamin A storage sites in rat liver. Exp. Cell Res. *160*, 138–149.

Hernandez-Gea, V., and Friedman, S.L. (2011). Pathogenesis of liver fibrosis. Annu. Rev. Pathol. *6*, 425–456.

Hua, S., Kittler, R., and White, K.P. (2009). Genomic antagonism between retinoic acid and estrogen signaling in breast cancer. Cell *137*, 1259–1271.

Inagaki, Y., and Okazaki, I. (2007). Emerging insights into Transforming growth factor beta Smad signal in hepatic fibrogenesis. Gut *56*, 284–292.

Janssens, W., Mathieu, C., Boonen, S., and Decramer, M. (2011). Vitamin D deficiency and chronic obstructive pulmonary disease: a vicious circle. Vitam. Horm. *86*, 379–399.

Kagan, H.M., and Li, W. (2003). Lysyl oxidase: properties, specificity, and biological roles inside and outside of the cell. J. Cell. Biochem. *88*, 660–672.

Kim, W.R., Brown, R.S., Jr., Terrault, N.A., and El-Serag, H. (2002). Burden of liver disease in the United States: summary of a workshop. Hepatology *36*, 227–242.

Knook, D.L., Seffelaar, A.M., and de Leeuw, A.M. (1982). Fat-storing cells of the rat liver. Their isolation and purification. Exp. Cell Res. *139*, 468–471.

Lee, U.E., and Friedman, S.L. (2011). Mechanisms of hepatic fibrogenesis. Best Pract. Res. Clin. Gastroenterol. *25*, 195–206.

Li, M.O., and Flavell, R.A. (2008). TGF-beta: a master of all T cell trades. Cell *134*, 392–404.

Li, Y.C., Pirro, A.E., Amling, M., Delling, G., Baron, R., Bronson, R., and Demay, M.B. (1997). Targeted ablation of the vitamin D receptor: an animal model of vitamin D-dependent rickets type II with alopecia. Proc. Natl. Acad. Sci. USA *94*, 9831–9835.

Lim, L.Y., and Chalasani, N. (2012). Vitamin d deficiency in patients with chronic liver disease and cirrhosis. Curr. Gastroenterol. Rep. *14*, 67–73.

Makishima, M., Lu, T.T., Xie, W., Whitfield, G.K., Domoto, H., Evans, R.M., Haussler, M.R., and Mangelsdorf, D.J. (2002). Vitamin D receptor as an intestinal bile acid sensor. Science *296*, 1313–1316.

Massagué, J. (2008). TGFbeta in Cancer. Cell *134*, 215–230.

Massagué, J., Seoane, J., and Wotton, D. (2005). Smad transcription factors. Genes Dev. *19*, 2783–2810.

Munger, K.L., Levin, L.I., Hollis, B.W., Howard, N.S., and Ascherio, A. (2006). Serum 25-hydroxyvitamin D levels and risk of multiple sclerosis. JAMA *296*, 2832–2838.

Nagpal, S., Na, S., and Rathnachalam, R. (2005). Noncalcemic actions of vitamin D receptor ligands. Endocr. Rev. *26*, 662–687.

Patsenker, E., and Stickel, F. (2011). Role of integrins in fibrosing liver diseases. Am. J. Physiol. Gastrointest. Liver Physiol. *301*, G425–G434.

Petta, S., Cammà, C., Scazzone, C., Tripodo, C., Di Marco, V., Bono, A., Cabibi, D., Licata, G., Porcasi, R., Marchesini, G., and Craxí, A. (2010). Low vitamin D serum level is related to severe fibrosis and low responsiveness to interferon-based therapy in genotype 1 chronic hepatitis C. Hepatology *51*, 1158–1167.

Ramagopalan, S.V., Dyment, D.A., Cader, M.Z., Morrison, K.M., Disanto, G., Morahan, J.M., Berlanga-Taylor, A.J., Handel, A., De Luca, G.C., Sadovnick, A.D., et al. (2011). Rare variants in the CYP27B1 gene are associated with multiple sclerosis. Ann. Neurol. *70*, 881–886.

Reynaert, H., Thompson, M.G., Thomas, T., and Geerts, A. (2002). Hepatic stellate cells: role in microcirculation and pathophysiology of portal hypertension. Gut *50*, 571–581.

Rosenbloom, J., Castro, S.V., and Jimenez, S.A. (2010). Narrative review: fibrotic diseases: cellular and molecular mechanisms and novel therapies. Ann. Intern. Med. *152*, 159–166.

Seki, E., De Minicis, S., Osterreicher, C.H., Kluwe, J., Osawa, Y., Brenner, D.A., and Schwabe, R.F. (2007). TLR4 enhances TGF-beta signaling and hepatic fibrosis. Nat. Med. *13*, 1324–1332.

Seki, E., and Schnabl, B. (2012). Role of innate immunity and the microbiota in liver fibrosis: crosstalk between the liver and gut. J. Physiol. *590*, 447–458.

Siegmund, S.V., Dooley, S., and Brenner, D.A. (2005). Molecular mechanisms of alcohol-induced hepatic fibrosis. Dig. Dis. *23*, 264–274.

Tanaka, A., Nezu, S., Uegaki, S., Kikuchi, K., Shibuya, A., Miyakawa, H., Takahashi, S., Bianchi, I., Zermiani, P., Podda, M., et al. (2009). Vitamin D receptor polymorphisms are associated with increased susceptibility to primary biliary cirrhosis in Japanese and Italian populations. J. Hepatol. *50*, 1202–1209.

Terrier, B., Carrat, F., Geri, G., Pol, S., Piroth, L., Halfon, P., Poynard, T., Souberbielle, J.C., and Cacoub, P. (2011). Low 25-OH vitamin D serum levels correlate with severe fibrosis in HIV-HCV co-infected patients with chronic hepatitis. J. Hepatol. *55*, 756–761.

Trompouki, E., Bowman, T.V., Lawton, L.N., Fan, Z.P., Wu, D.C., DiBiase, A., Martin, C.S., Cech, J.N., Sessa, A.K., Leblanc, J.L., et al. (2011). Lineage regulators direct BMP and Wnt pathways to cell-specific programs during differentiation and regeneration. Cell *147*, 577–589.

Tsukada, S., Parsons, C.J., and Rippe, R.A. (2006). Mechanisms of liver fibrosis. Clin. Chim. Acta *364*, 33–60.

Vadasz, Z., Kessler, O., Akiri, G., Gengrinovitch, S., Kagan, H.M., Baruch, Y., Izhak, O.B., and Neufeld, G. (2005). Abnormal deposition of collagen around hepatocytes in Wilson's disease is associated with hepatocyte specific expression of lysyl oxidase and lysyl oxidase like protein-2. J. Hepatol. *43*, 499–507.

von Essen, M.R., Kongsbak, M., Schjerling, P., Olgaard, K., Odum, N., and Geisler, C. (2010). Vitamin D controls T cell antigen receptor signaling and activation of human T cells. Nat. Immunol. *11*, 344–349.

Williams, R. (2006). Global challenges in liver disease. Hepatology *44*, 521–526.

Wynn, T.A. (2008). Cellular and molecular mechanisms of fibrosis. J. Pathol. *214*, 199–210.

Xu, L., Hui, A.Y., Albanis, E., Arthur, M.J., O'Byrne, S.M., Blaner, W.S., Mukherjee, P., Friedman, S.L., and Eng, F.J. (2005). Human hepatic stellate cell lines, LX-1 and LX-2: new tools for analysis of hepatic fibrosis. Gut *54*, 142–151.

Yoshiji, H., Kuriyama, S., Yoshii, J., Ikenaka, Y., Noguchi, R., Nakatani, T., Tsujinoue, H., Yanase, K., Namisaki, T., Imazu, H., and Fukui, H. (2002). Tissue inhibitor of metalloproteinases-1 attenuates spontaneous liver fibrosis resolution in the transgenic mouse. Hepatology *36*, 850–860.